Improvement of the Intranuclear Cascade code of Bruyères-le-Châtel (BRIC) at low intermediate energy

Helder Duarte
CEA Bruyères-le-Châtel, DIF/DPTA/Service de Physique Nucléaire,
B.P. 12, F-91680 Bruyères-le-Châtel, France
e-mail : helder.duarte@cea.fr

Abstract : The IntraNuclear Cascade code of Bruyères-le-Châtel called BRIC has been extended to low intermediate energy by taking in account some medium effects that are included in other nuclear dynamics models such as BUU or QMD. We present the results of BRIC 1.0 without the medium effect and of BRIC 1.4 with the medium effects on a wide range of incident energy. The medium effects correct the main discrepancies that appear at low intermediate energy with BRIC 1.0 and do not damage the good results at high energy. The good agreement of the results of BRIC 1.4 with data allows to conclude that no preequilibrium model is necessary between our INC and the deexcitation step.

1 Introduction

More than fifty years ago Serber [1] suggested that the inelastic nuclear reactions induced by high energy particles (nucleon, pion or light nucleus) on nuclei should be divided in fast and slow steps. High energy particles are emitted throughout the fast step and an excited nucleus is formed at the end. The deexcitation of the compound nucleus is then done in the second step. This approach is the basis of the intranuclear cascade (INC) + deexcitation models and of the preequilibrium + deexcitation models. The deexcitation step is often viewed as a competition between the evaporation of nucleons and light nuclei, the fission and/or the fragmentation, and the gamma decay.

An application field of codes of inelastic reaction is their use as event generator of spallation reactions in macroscopic transport codes like MCNPX [2] for instance. Indeed due to the high number of final channels in particle-nucleus interaction at intermediate energy, the large number of differential cross sections of particle production are not stored in databases but are calculated "on-line" by nuclear models.

Even if the INC models and some preequilibrium models may present strong similarities, they differ on numerical approach: the time-space treatment of the binary collisions of two hadrons in the nuclear volume requires a Monte-Carlo method in the INC model while the preequilibrium models do not necesserally use stochastic method. Their respective range of the incident energy are also different: the INC approach takes into account the production of other hadrons than the nucleons and works well at high energy up to tens of GeV, its results are however in poor agreement with data at low intermediate energy (below 300 MeV typically) [3, 4, 5], while the upper energy limit of the preequilibrium models is often the pion production threshold.

Other sophisticated nuclear dynamics models such as BUU [6], BNV [7], QMD [8] are carried out since many years to simulate heavy ion reaction above the Fermi energy. They overtook the INC model in the Fermi energy range in heavy ion physics [9] since they deal with the generation and evolution of the mean field self-consistently. Their results are also in good agreement with experimental data in the spallation field (see [10, 11, 12] for the QMD model) at high and low intermediate energy. However their computing time is very large compared to INC codes, it then limits their use in high energy transport codes to simulate inelastic reactions in macroscopic targets. From this point of view the INC's remain the most interesting tools for the simulation of high energy inelastic reaction.

One way to improve the results of INC+evaporation at intermediate energy is to insert a preequilibrium step between the INC and the evaporation [13]. Another way is to improve the physics straight in INC at low intermediate energy. For that we may take into account some of the features of these sophisticated nuclear dynamics models, even if they are not fully quantum. One feature concerns the medium effect implicitly included in their modelisation: the equations of motion and the mean field. Another one has already been investigated in heavy ion physics field: the in-medium cross sections. The best way to constrain the INC model is to study low intermediate energy reactions. We may then expect that the improvements of the INC done at low intermediate energy work also at higher energy.

In the first section, we describe the INC of Bruyères-le-Châtel without (BRIC 1.0) and with some medium effects (BRIC 1.4). Then the results of the two approaches are compared to data from low to high incident energy and discussed.

2 Description of the BRIC code

The reference [14] provides a description of BRIC 1.0. We recall here its main features and we detail the changes that are done in BRIC 1.4.

2.1 Initialisation of the system

The relativistic kinematics is used to keep the energy-momentum conservation at the binary collisions since the range of the incident energy extends up to a few GeV. In the present work the hadrons are restricted to nucleons, pions and Δ resonances with their isospin degree of freedom. They are modelized by points in phase space with classical trajectories. The treatment and then the emission of clusters (d, .. α) are not included for the moment.

The target nucleus is a spherical cloud of individual nucleons inside a potential well $V(r)$ centered at the origin of the laboratory frame. The positions of these nucleons are randomly sampled from a Woods-Saxon function :

$$\rho(r) = \frac{\rho_0(A)}{1 + \exp\frac{r - R(A)}{a(A)}}. \tag{1}$$

The mean radius R and the diffuseness a of stable nuclei come from the fit of this Woods-Saxon function on Hartree-Fock-Bogoliubov calculations [15]. The conservation law $4\pi \int \rho(r)\, r^2\, dr = A$ gives $\rho_0(A)$. Once the position $\vec{r}$ is defined, the momentum of the target nucleon is chosen isotropically in the sphere of a radius equal to the local Fermi momentum $p_F(r) \sim [2m(V(r) - e_{bind})]^{1/2}$, e_{bind} being the binding energy per nucleon.

The hadrons are divided in 2 groups : the spectator (or bound) nucleons and the quasi-free hadrons. The quasi-free hadrons are the nucleons of kinetic energy greater than the local potential $|V(r)|$, the pions or the Δ resonances. The spectator nucleons are all the other nucleons. A spectator nucleon goes in the quasi-free state after a collision if its final energy is greater than $|V(r)|$, and reciprocally a quasi-free nucleon goes in the spectator state if its final energy is less than $|V(r)|$. The incident nucleon (or pion) is the only quasi-free hadron at the start of the inelastic reaction, and no collision occurs between spectator nucleons.

We now define the potentials, the equations of motion and the nucleon-nucleon cross sections that are used in the two approaches.

2.2 Potential

The following potentials are taken into account in the energy balance at any time.

In BRIC 1.0, the potential shape comes from the Fermi gas model:

$$V(r) = V_0(A)\left(\frac{\rho(r)}{\rho_0(A)}\right)^{2/3}.$$

The amplitude $V_0(A)$ of the potential well increases linearly with the mass number A through $V_0(12) = -32.5$ MeV and $V_0(208) = -45$ MeV. The protons, neutrons and Δ's share the same potential, and the pions have no potential. The Coulomb potential is not explicitly taken into account in energy balance. However it enters in the calculation of the transmission coefficient of quasi-free charged hadrons when they leave the nuclear volume. The probability to reflect a charged hadron back inside the nucleus is given by a Gamow factor [16].

In BRIC 1.4, the potential $V(r)$ is close to a Skyrme parametrisation and includes the Coulomb field now:

$$V(r) = V_N(r) + V_C(r) = V_0\left(\frac{\rho(r)}{\rho_0(A)}\right)^{2/3} + V_C(r). \qquad (2)$$

The amplitude V_0 of $V_N(r)$ is independant of the mass A and is equal to -48 MeV for the baryons (nucleons and Δ's), and to 0 for the pions. The Coulomb potential $V_C(r)$ is updated when a charged hadron goes out. The transmissions coefficient for all quasi-free hadrons are calculated with $V(r)$ in the WKB approximation.

2.3 Equation of motion

We now define the time evolution of the positions and momenta $\{\vec{r_i}(t), \vec{p_i}(t)\}$ of the quasi-free hadrons in the phase space.

In BRIC 1.0 their trajectories between two collisions are approximated by straight lines, the energy conservation $E+V$ is nevertheless required. We do not write the corresponding equations of motion since they may not easily read. This approximation, which is almost acceptable for very high energy particles, is extended to all quasi-free hadrons to get a low computing time.

In BRIC 1.4 the equations of motion of the quasi-free hadrons are:

$$\begin{aligned} \frac{d\vec{p}}{dt} &= -\vec{\nabla} V \\ \frac{d\vec{r}}{dt} &= \frac{\vec{p}}{E} \end{aligned}$$

where E is the total relativistic energy of the hadron. Their trajectories are curvilign between 2 time steps and the time step is 1 fm/c. The binary collisions are inserted between 2 time steps as we describe now.

2.4 Nucleon-Nucleon cross sections

The time and position of the collision of two hadrons i and j are determined by a condition on their distance of minimal approach: $Min(|\vec{r_i} - \vec{r_j}|) < \sqrt{\sigma_{ij}/\pi}$, σ_{ij} being the total cross section at the center of mass energy $\sqrt{s_{ij}}$. One of the two hadrons at least must be in a quasi-free state. The total cross sections are divided in elastic and inelastic cross sections.

In BRIC 1.0 the np and pp elastic cross sections are parametrisations fitted on the experimental data (see blue curves in figure 1).

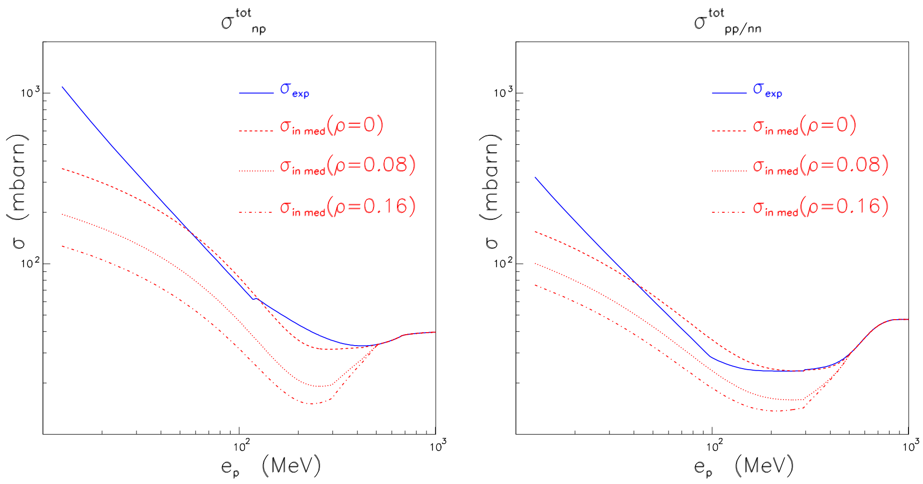

Figure 1: Total cross section of np (right) and pp (left) scattering. The blue curves are the parametrisations fitted experimental data and used in BRIC 1.0. The red curves are the density dependant parametrisations of Li and Machleidt [17] up to 300 MeV and our linear interpolation between 300 and 500 MeV. These parametrisations are used in BRIC 1.4.

In BRIC 1.4 we use the parametrisations of the in-medium cross sections of Li and Machleidt up to 300 MeV [17]. They are deduced from $\tilde{G}$ matrix calculation in the nuclear matter in the Dirac-Brueckner approach, and do not include the Pauli blocking factor for the final states. We interpolate the elastic cross sections between 300 and 500 MeV. The in-medium cross sections decrease with increasing density ρ (see red curves in figure 1).

Other cross sections are identical in BRIC 1.0 and 1.4. The πN cross sections are the experimental ones and $\sigma(N\Delta \to NN)$ is deduced from $\sigma(NN \to N\Delta)$ by the detailed balance principle.

2.5 Collision

The momenta of hadrons after collision are defined by random azimuthal and polar angles in the center of mass frame according to differential cross section and energy-momentum conservation as in other INC models [18]. The differential cross sections of np and pp elastic scattering are parametrisations adjusted on the experimental data [14]. The differential cross section of $np \to N\Delta$ is the one proposed by Cugnon *et al.* [19]. The Δ is assumed to decay in P-wave. The isospin conservation is applied at each collision and decay.

After a hadron-hadron collision or a Δ decay, the Pauli exclusion principle is applied on the final nucleons. We define a sharp cut-off Pauli blocking : the collision or the decay is authorized only if $p_i > p_F(r_i)$, where $\vec{p_i}$ is the momentum of nucleon i after the process, and $p_F(r_i)$ is the local Fermi momentum of the nucleon i. The main reason of this choice is that an high energy quasi-free nucleon see an unperturbed nucleus in first approximation, all bound states being occupied. If the kinetic energy of a nucleon after a collision or after a Δ decay falls in the gap between the Fermi energy and the amplitude of potential $|V(r)|$, this nucleon is "frozen" and becomes spectator.

2.6 Conservation laws and end of the INC

We have now to define the end of the INC step.

The time approach in our INC model allows to define some global quantities as function of

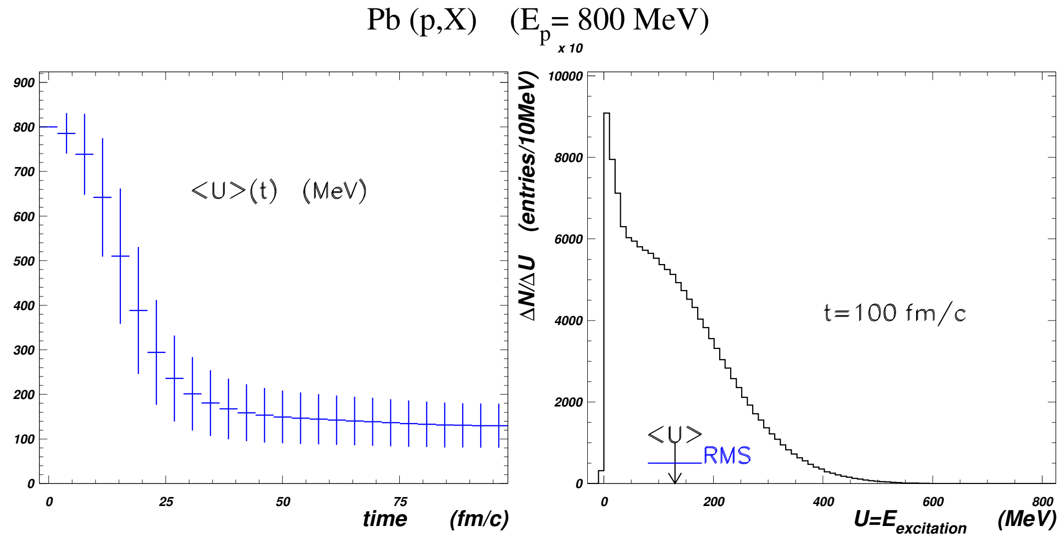

Figure 2: Distribution $\Delta N/\Delta U_{exc}$ of the excitation energy U_{exc} at time t=100 fm/c (right), and distribution of the mean excitation energy $<U_{exc}>(t)$ as a function of time t (left). The vertical blue bars in the left plot are the root mean square (RMS) of $\Delta N/\Delta U_{exc}$.

the time. The mass, charge, recoil momentum, angular momentum and excitation energy of the nuclear system are thus determined by conservation laws. One of the most interesting quantity for our purpose is the excitation energy of the nuclear system projectile+target. One way to calculate this energy at any time is to substract the energies of outgoing particles from the initial energy:

$$U_{exc}(t) = e_{inc} + \delta_{inc\ \pi} m_\pi + (1 - \delta_{inc\ \pi}) e_{bind} - \left(\sum_{i=1}^{x_N(t)} (e_i + e_{bind}) + \sum_{j=1}^{x_\pi(t)} (e_j + m_\pi) \right) - E_{rec} \quad (3)$$

where e_{inc}, e_i and e_j are the kinetic energies of the incident hadron, and of the emitted nucleon i and pion j, respectively. $x_N(t)$ and $x_\pi(t)$ are the numbers of emitted nucleon and pion before time t, respectively. e_{bind} is the binding energy per nucleon and m_π is the pion mass. $\delta_{inc\ \pi} = 0$ for an incident nucleon, and $\delta_{inc\ \pi} = 1$ for an incident pion. The recoil energy of the residual nucleus E_{rec} comes from the momentum conservation.

In order to define the end of the INC, we study the distribution of the mean excitation as a function of the time for a lot of reactions. The mean excitation distribution comes from the average of $U_{exc}(t)$ on a large number of events. The right plot of the figure 2 shows for instance the distribution of the excitation energy $U_{exc}(t = 100)$ at time 100 fm/c for the $Pb(p, x)$ reaction at 800 MeV given by BRIC 1.0. The mean excitation $<U_{exc}>$ (100 fm/c) is indicated on the plot, the blue bar is the root mean square (RMS) of the distribution. The left plot of figure 2 presents the values of $< U_{exc} >$ and RMS every 4 fm/c.

With the sharp cut-off Pauli blocking and the "freezing" of nucleon of kinetic energy lower than $|V(r)|$, $<U_{exc}>$ is almost constant between 50 and 100 fm/c for this reaction. This result of BRIC 1.0 is confirmed with BRIC 1.4 and for all hadron induced reactions above 40 MeV. We decide to stop the cascade event at t_{cut} = 100 fm/c. QMD calculations show also that this time is enough to treat the fast step of a spallation reaction [11].

In the next section we present the results of our two INC approaches, BRIC 1.0 without medium effects and BRIC 1.4 with the medium effects: the realistic equations of motion, the potential with coulomb field and the in-medium NN cross sections. We will show comparisons to experimental data, and discuss some points.

3 Results of the two approaches and discussion

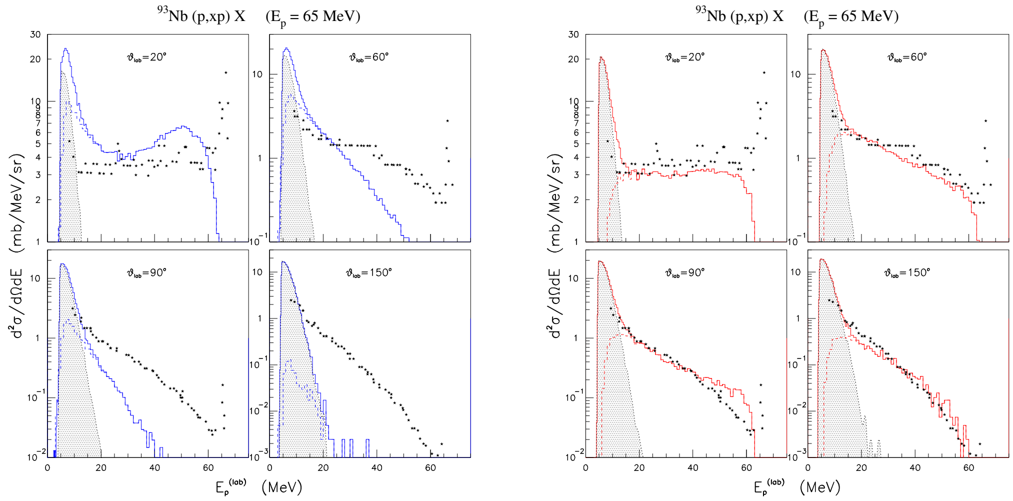

Figure 3: Differential cross section for the reaction of 65 MeV proton on ^{93}Nb as a function of the energy of the outgoing proton for the angles indicated. The fill area, the hashed histograms and the solid histograms are the evaporation component, the INC component and the INC+evaporation sum, respectively. The left figure (blue histograms) shows the results of the BRIC code without the medium effects (BRIC 1.0), the right figure (red histograms) is the same for the BRIC code with the medium effects presented in this paper (BRIC 1.4). The data are from [22].

Since the INC is viewed as the first step of a deep inelastic reaction, the most relevant data to test only an INC model is the double differential cross sections of particle production of high energy as function of the energy (or the detection angle) of the outgoing particle at some emission angles (or some outgoing energies). The energy of the outgoing particle has to be greater than a few tens of MeV to be sure that it comes from the first step of the reaction and not from the deexcitation step. The differential cross section of production of high energy particle and the correlations of two or three outgoing particles are also useful to the INC study.

Another useful data are the cross sections of production of residual nuclei. However they depend not only on the mass, charge and excitation energy at the end of the INC but also on the parameters of the deexcitation model. In this paper we only show results of double differential cross sections of nucleon production.

However some experimental data are sometimes available up to low energy of the outgoing nucleon. In order to do comparison, our cascade code BRIC has been linked to an evaporation in competition with fission and fragmentation. The mass, charge, excitation energy and recoil momentum of the remaining nucleus at the end of the INC are transmitted to the evaporation which is the main link of the deexcitation for the results presented here. Our Monte-Carlo evaporation code is based on the statistical approach of Weisskopf-Ewing [20]. The calculation of the partial widths of the emission of nucleons and light nuclei uses the energy dependent level density parametrisation of Ignatyuk *et al* [21].

The figure 3 shows the double differential cross section of proton production for the reaction of 65 MeV proton on ^{93}Nb. The left and right plots present the results of the BRIC code without and with the medium effects, respectively. In each plot the fill area, the hashed histogram and the solid hitogram are the evaporation component, the INC component and the sum INC+evaporation, respectively. In comparison to the data the main discrepancies of BRIC 1.0 are the overestimated peak at very forward angle and the too large anisotropy of the proton

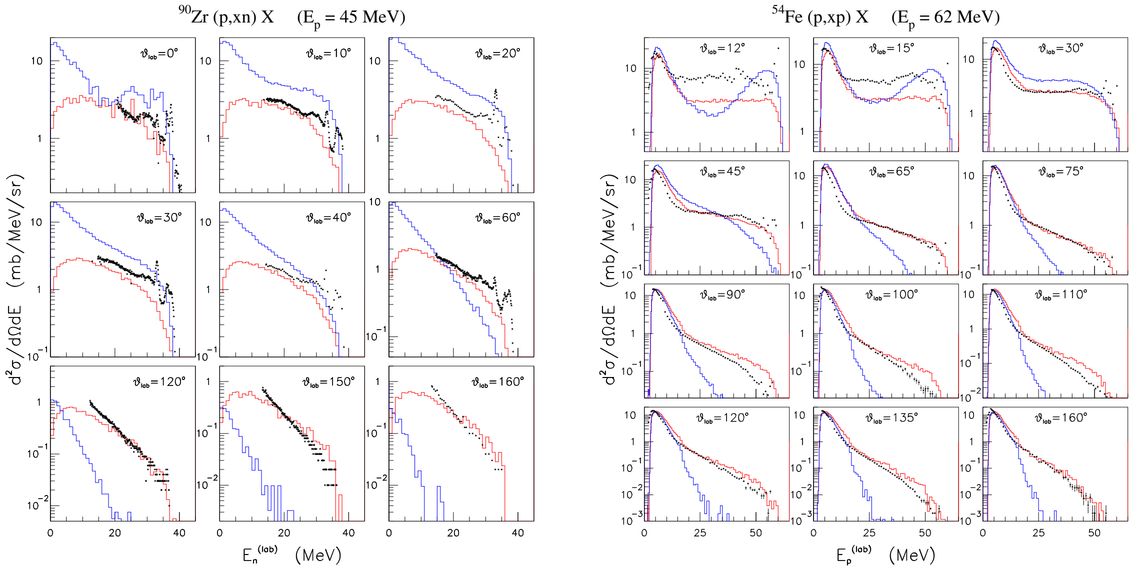

Figure 4: Differential cross section for the reaction of 45 MeV proton on ^{90}Zr (left figure) and of 62 MeV proton on ^{56}Fe (right figure) as a function of the energy of the outgoing neutron and proton, respectively, for the angles indicated. The blue histograms are the results of the code BRIC 1.0 and the red histograms those of BRIC 1.4. The calculation of $^{56}Fe(p,xp)$ includes the evaporation. The data of $^{90}Zr(p,xn)$ and $^{56}Fe(p,xp)$ are from [23] and [3], respectively.

production that gives the underproduction at backward angles. These discrepancies appear in other reactions (see the $^{56}Fe(p,xp)$ reaction of figure 4) and at higher incident energies. And they have already been observed with previous INC models [3, 4, 23].

Taking into account the medium effects (BRIC 1.4) really improves the results as we see the red histograms in figure 3 (right plots). After the analysis of the sequence of the INC, we can say that the flat distribution in (p,xp) reaction at forward angles comes mainly from the equations of motion that are more realistic in BRIC 1.4 than in BRIC 1.0. On the other hand the better agreement of the calculations with data at intermediate and backward angles is the result of the three modifications together: the equations of motion, the NN cross sections and the new potential (2). However INC is not able to reproduce the thin structures of the differential cross sections since the bound nucleons are distributed in phase space according to a Fermi gas and that no nuclear level is taken into account.

The figure 4 presents two other calculations at low intermediate energy. The neutron production for the reaction of 45 MeV proton on ^{90}Zr is improved specially at backward angles with BRIC 1.4 (red histograms) in comparison to BRIC 1.0 (blue histograms), again thanks to the medium effects. For the reaction $^{54}Fe(p,xp)$ at 62 MeV, the shape of distribution of outgoing protons is correct with BRIC 1.4 but the amplitude is too small at forward angles. Above 30^o (and even 20^o see figure 3) the spectra are in good agreement with the data. We have seen this discrepancy with other reactions at low intermediate energy. No explanation has been found for the moment.

We have verified on the available (p,xp) and (p,xn) data between 40 MeV and 250 MeV that the same improvement of the results occur at very forward and backward angles when the medium effects are taken into account. The figure 5 present examples of the double differential cross sections of proton production as functions of the laboratory angle at the indicated outgoing energies. The histograms are the results of BRIC alone (without evaporation). The agreement with data is clearly better with BRIC 1.4 (red histograms) than with BRIC 1.0 (blue

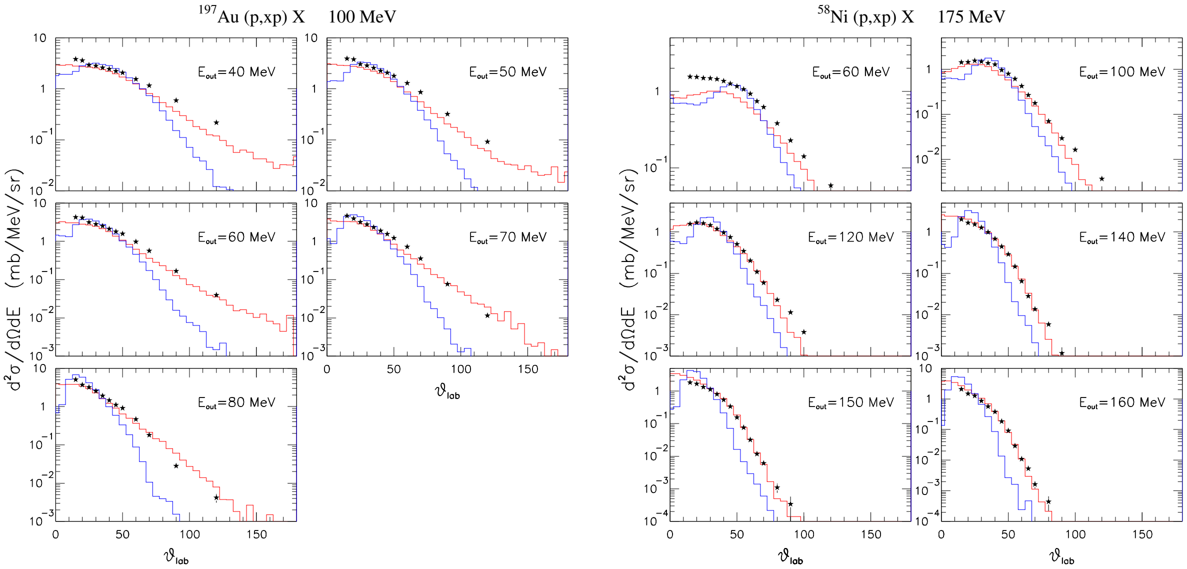

Figure 5: Differential cross section for the reactions $^{197}Au(p,xp)$ at 100 MeV (left figure) and $^{58}Ni(p,xp)$ at 175 MeV (right figure) as a function of the laboratory angles of the outgoing protons for the energies indicated. The experimental data (stars) are from Richter *et al.* [24]. The blue histograms are the results of BRIC 1.0 only (no evaporation) and the red histograms those of BRIC 1.4 only.

histograms). Same conclusion with the neutron production in 113 MeV proton induced reactions (not shown here) and in 256 MeV proton induced reactions (see figure 6 for $^{56}Fe(p,xn)$ reaction). In the reaction $^{56}Fe(p,xn)$ at 256 MeV, the separation of the BRIC component and of the evaporation component that are not shown in the figure proves that the production of neutron of energy less than 20-30 MeV is more isotropic with BRIC 1.4 than with BRIC 1.0. Indeed the realistic equations of motion correct the emission angle of low energy neutrons and then the overproduction at 7.5°, 30° and 60° that appears in the BRIC 1.0 results (blue histograms).

Above around 600 MeV, the results of BRIC 1.0 and BRIC 1.4 are almost identical. The right figure 6 and the figures 7 show the same kind of double differential cross section than the reaction $^{56}Fe(p,xn)$ at 256 MeV. The changes in the results of BRIC without and with the medium effects are less and less impressive when the incident energy increases. We could have expected it since the medium effect on the trajectories and the NN cross sections are stronger for hadrons below 400 MeV and when their energy decreases than for high energy hadrons. However we were not able to predict if the distribution of (A,Z,Eexc) at the end of INC would be strongly modified or not. The components of neutron evaporation seem almost similar in the two approaches and are in good agreement with the data. That means the distribution of (A,Z,Eexc) at t=100 fm/c is not strongly modified on average.

At 597 MeV we added the results of BRIC at the angle 7.5° to show that the quasi-elastic peak (p,n) at very forward is changed thanks to the equation of motion even at higher energies than 256 MeV. This correction of the quasi-elastic peak goes on until 800 MeV incident energy and is slighter at 1200 MeV. Moreover an improvement of the outgoing neutrons at backward angles is noticeable in figures 6 and 7. We may conclude that the medium effects at least do not introduce any discrepancy at high energy but can even improve the results.

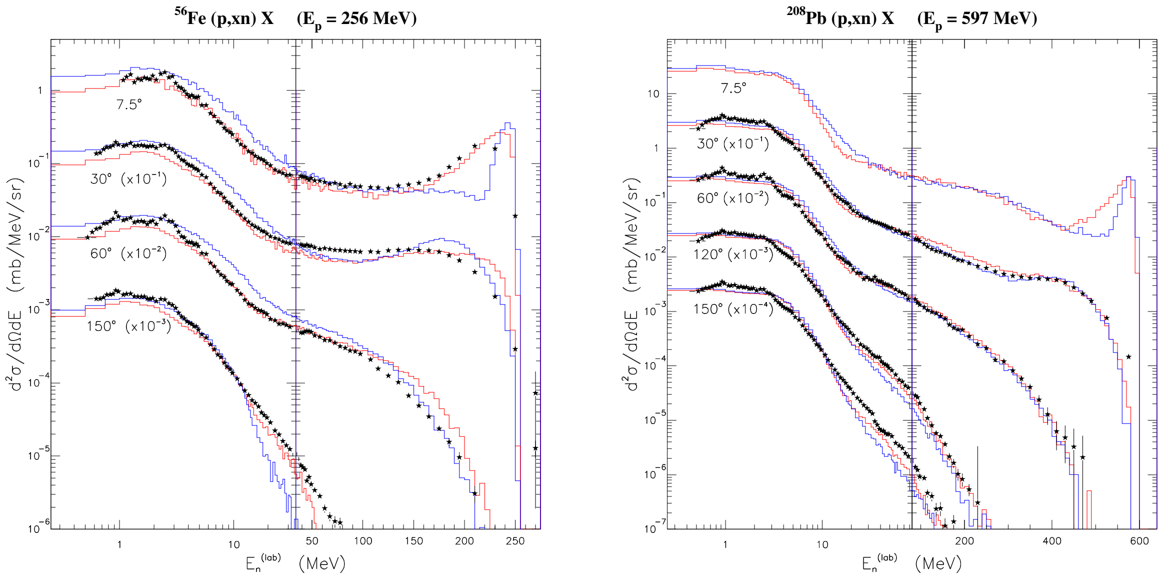

Figure 6: Differential cross section for the reactions $^{56}Fe(p,xn)$ at 256 MeV (left figure) and $^{208}Pb(p,xn)$ at 597 MeV (right figure) as a function of the energy of the outgoing neutrons for the angles indicated. The results of two angles are shifted by a 0.1 factor. They are given in the laboratory frame. Each figure is divided in two parts, the low energy part has a logarithmic-logarithmic scale, the high energy has a linear-logarithmic scale. The blue and red histograms are the results of BRIC 1.0 and BRIC 1.4, respectively, plus the evaporation. The data at 256 MeV and at 597 MeV are from [5] and [25], respectively. No data is available at 7.5^o for the reaction of 597 MeV proton on ^{208}Pb.

4 Conclusion

The computing times of BRIC 1.0 and 1.4 are low in comparison to nuclear dynamics models like BUU and QMD: one or several million inelastic events can be calculated in 1 hour on one current medium CPU according to the nucleus mass A. We have intentionnally done approximations to keep this CPU time enough low to use it as an event generator for macroscopic transport codes. But as we have shown the approximation of linear trajectories should not be kept. Realistic equations of motion implicitly included in nuclear dynamics models like BUU and QMD are accessible to INC model without a large increase of the CPU time (BRIC 1.4 is less than 3 times slower than BRIC 1.0). Other physics effects included in these models should not be so easily implemented in INC model with low computing time. It should be the case of the time evolution of the nuclear mean field which is almost fixed in our approach. However this last point is more crucial in heavy ion collisions than in hadron induced reactions.

The medium effects presented in this paper are important at low and intermediate incident energy as one could have expected. Moreover, even if they are less impressive at high energy, they do not damage the good agreement of the results with data at high energy. One important conclusion is that no preequilibrium model seems necessary between our INC with medium effects and the deexcitation step.

References

[1] R. Serber, Phys. Rev. **72**, 1008 (1947).
[2] M.B. Chadwick *et al.* Nucl. Sci. Eng. **131**, 293 (1999).
[3] F.E. Bertrand and R. Peele, Phys. Rev. **C 8**, 1045 (1973).

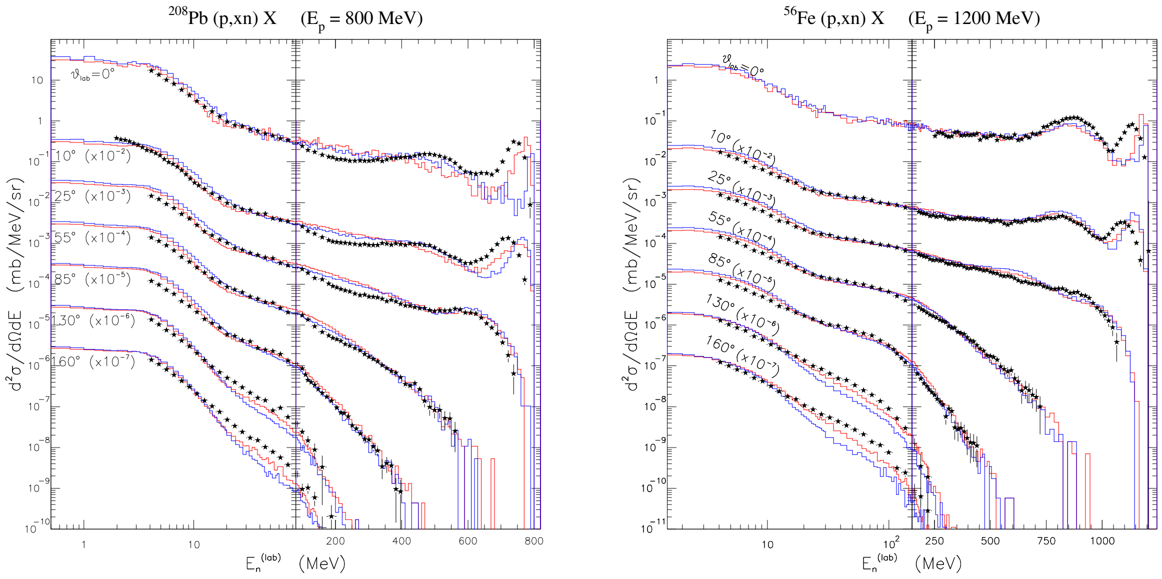

Figure 7: Same as in fig. 6 for 800 MeV proton on ^{nat}Pb (left plot) and for 1200 MeV proton on ^{56}Fe (right plot). The data are from [26].

[4] H.W. Bertini, G.D. Harp and F.E. Bertrand, Phys. Rev. **C 10**, 2472 (1974).

[5] M.M. Meier *et al.*, Nucl. Sci. Eng. **110**, 289 (1992).

[6] G.F. Bertsch and S. Das Gupta, Phys. Rep. **160**, 189 (1988).

[7] A. Bonasera, F. Gulminelli and J. Molitoris, Phys. Rep. **243**, 1 (1994).

[8] J. Aichelin, Phys. Rep. **202**, 233 (1991)

[9] H. Stöcker and W. Greiner, Phys. Rep. **137**, 277 (1986).

[10] G. Peilert *et al.*, Phys. Rev. **C46**, 1457 (1992).

[11] K. Niita *et al.*, Phys Rev. **C 52**, 2620 (1995).
M.B. Chadwick *et al.* , Phys Rev. **C 52**, 2800 (1995).

[12] S. Chiba *et al.*, Phys Rev. **C 53**, 1824 (1996).

[13] K.K. Gudima, S.G. Mashnik and V.D. Toneev, Nucl. Phys. **A401**, 329 (1983).

[14] H. Duarte, *contribution to the proceedings of the Third International Conference on Accelerator-Driven Transmutation Technologies and Applications* (Praha, Czech Republic, June 7-11 (1999)), *http://www.fjfi.cvut.cz/con_adtt99/papers/Mo-o-c17.pdf.*

[15] J.F. Berger, M. Girod and D. Gogny, Comput. Phys. Commun. **63**, 365 (1990) and references therein.

[16] J. Cugnon, C. Vollant and S. Vuillier, Nucl. Phys. **A 620**, 475 (1997).

[17] G.Q. Li and R. Machleidt, Phys. Rec. **C 48**, 1702 (1993); Phys. Rec. **C 49**, 566 (1994).

[18] J. Cugnon, Nucl. Phys. **A 462**, 751 (1987).

[19] J. Cugnon *et al.*, Phys. Rev. **C 56**, 2431 (1997).

[20] V. F. Weisskopf and D. H. Ewing, Phys. Rev. **57** (1940) 472.

[21] A.V. Ignatyuk, G.N. Smirenkin and A.S. Tishin, Sov. J. Nucl. Phys. **21**, 255

[22] H. Sakai *et al.* Nucl. Phys. **A 344**, 41 (1980).

[23] A. Galonsky *et al.*, Phys. Rev. **C 14**, 748 (1976).

[24] W.A. Richter *et al.*, Phys. Rev. **C 46**, 1030 (1992).

[25] W.B. Amian *et al.*, Nucl. Sci. Eng. **115**, 1 (1993).

[26] S. Leray *et al.*, Phys. Rev. **C 65**, 044621 (2002).